ACS APPLIED MATERIALS & INTERFACES

Research Article

www.acsami.org

Strong Electroactive Biodegradable Shape Memory Polymer Networks Based on Star-Shaped Polylactide and Aniline Trimer for Bone Tissue Engineering

Meihua Xie,[†,∇] Ling Wang,[†,∇] Juan Ge,[†] Baolin Guo,*[,†] and Peter X. Ma*[,†,‡,§,∥,⊥]

[†]Center for Biomedical Engineering and Regenerative Medicine, Frontier Institute of Science and Technology, Xi'an Jiaotong University, Xi'an, 710049, China

[‡]Department of Biomedical Engineering, University of Michigan, Ann Arbor, Michigan 48109, United States

[§]Department of Biologic and Materials Sciences, University of Michigan, 1011 North University Avenue, Room 2209, Ann Arbor, Michigan 48109, United States

[∥]Macromolecular Science and Engineering Center, University of Michigan, Ann Arbor, Michigan 48109, United States

[⊥]Department of Materials Science and Engineering, University of Michigan, Ann Arbor, Michigan 48109, United States

Supporting Information

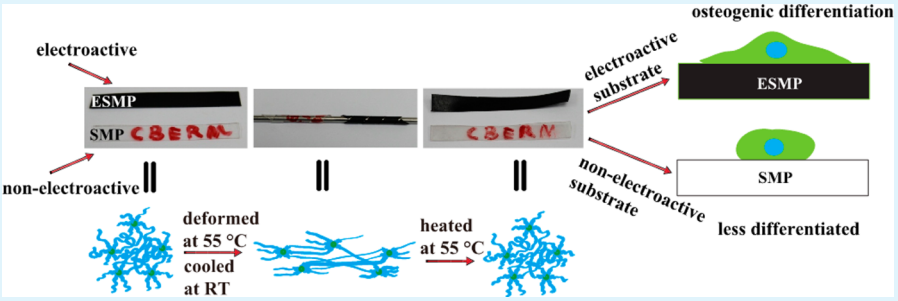

ABSTRACT: Preparation of functional shape memory polymer (SMP) for tissue engineering remains a challenge. Here the synthesis of strong electroactive shape memory polymer (ESMP) networks based on star-shaped polylactide (PLA) and aniline trimer (AT) is reported. Six-armed PLAs with various chain lengths were chemically cross-linked to synthesize SMP. After addition of an electroactive AT segment into the SMP, ESMP was obtained. The polymers were characterized by ^{1}H NMR, GPC, FT-IR, CV, DSC, DMA, tensile test, and degradation test. The SMP and ESMP exhibited strong mechanical properties (modulus higher than GPa) and excellent shape memory performance: short recovery time (several seconds), high recovery ratio (over 94%), and high fixity ratio (almost 100%). Moreover, cyclic voltammetry test confirmed the electroactivity of the ESMP. The ESMP significantly enhanced the proliferation of C2C12 cells compared to SMP and linear PLA (control). In addition, the ESMP greatly improved the osteogenic differentiation of C2C12 myoblast cells compared to PH10 and PLA in terms of ALP enzyme activity, immunofluorescence staining, and relative gene expression by quantitative real-time polymerase chain reaction (qRT-PCR). These intelligent SMPs and electroactive SMP with strong mechanical properties, tunable degradability, good electroactivity, biocompatibility, and enhanced osteogenic differentiation of C2C12 cells show great potential for bone regeneration.

KEYWORDS: *shape memory polymers, conducting polymers, bone tissue engineering, osteogenic differentiation, polylactide*

1. INTRODUCTION

Shape memory polymer (SMP) is a smart material capable of fixing temporary shape and reverting to the memorized permanent shape when exposed to stimuli. This notable material has been applied in various biomedical areas, such as sutures,[1] cardiovascular stents,[2] drug-eluting stents,[3] and implants for invasive surgery.[2,4] Thermally induced shape memory polymer is one outstanding class of SMPs which is triggered by heat. A series of thermally induced SMP based on polylactide (PLA) was reported due to the good biocompatibility and degradability of PLA.[5−8] But some limitations still exist in the systems, such as low fixity ratio, low modulus, and long recovery time. Jianwen Xu and Jie Song developed a high performance SMP based on a polyhedral oligomeric silsesquioxane (POSS) nanoparticle which was a rigid core and imparted good shape memory properties. However, the nanoscale POSS possesses some drawbacks, such as heterogeneous dispersion, poor biostability *in vitro*,[9] and the unsure biosecurity of the nanoparticles. In contrast, inositol with six hydroxyl groups has been found ubiquitously in the biological

Received: January 9, 2015
Accepted: March 5, 2015
Published: March 5, 2015

DOI: 10.1021/acsami.5b00191
ACS Appl. Mater. Interfaces 2015, 7, 6772−6781

kingdom. It plays very important roles in membrane biosynthesis, stress responses, growth regulation and many other processes, and it is safe for humans.[10] The inositol, a cyclic rigid core, enables the grafting of six polymer arms to form a star-shaped macromolecule. It is therefore desirable to design the shape memory polymer network based on the star-shaped polylactide with inositol as the core.

Many researchers reported the electrical signals could regulate a range of cellular activities, such as cell adhesion, migration, proliferation, DNA synthesis, and so on.[11,12] Therefore, electrically conductive materials such as polyaniline (PANI), polypyrrole (PPy), and other conductive nanoparticles have been widely developed as conductive matrixes in tissue engineering.[13−17] But the poor mechanical properties, non-degradability, poor solubility, and bad processability of conducting polymers restrict their biomedical applications.[18,19] In contrast to the PANI, aniline oligomers characteristically have good electroactivity, biodegradability, and good processing properties, and they can be copolymerized with other degradable polymers.[20−29] Many reports showed amino-capped aniline trimer (AT) had a well-defined electroactive structure, good processability, and ease of degradability.[30,31] We anticipated that by incorporating an electroactive AT segment into shape memory polymers, we could obtain electroactive degradable polymeric materials with shape memory properties, which will greatly expand their biomedical applications.

The aim of this work was to design an electroactive degradable shape memory polymer network based on star-shaped polylactide and amino-capped aniline trimer, and to demonstrate their potential application for bone tissue engineering. We incorporated the electroactive aniline trimer into star-shaped PLAs with HDI as cross-linker and coupling reagent to endow electroactivity to the SMP. The synthesis, thermal properties, mechanical properties, thermal mechanical properties, degradability, electroactive properties, shape memory properties, and biocompatibility of these electroactive SMPs (ESMPs) were investigated. The ESMPs showed good electroactivity, strong mechanical properties, good shape memory properties, and tunable degradability. We further demonstrated that the EMSPs could greatly enhance the C2C12 cell proliferation and showed a higher ability to induce the osteogenic differentiation of C2C12 cells than polylactide in terms of the expression of alkaline phosphatase (ALP) mRNA, ALP activity, and osteogenesis marker protein Runt-related transcription factor 2 (RUNX2). Due to the strong mechanical properties, good shape memory property, and electroactivity of the ESMPs, they are good candidates for bone tissue engineering.

2. EXPERIMENTAL SECTION

2.1. Materials. L-Lactide (LLA) was purified in dry toluene by recrystallization and subsequently dried under reduced pressure (10^{-2} mbar) for at least 48 h at room temperature prior to polymerization. Aniline (J&K Scientific Ltd.) was distilled twice under reduced pressure before use. Stannous octoate, $Sn(Oct)_2$, from Aldrich was dried over molecular sieves and kept at a N_2 atmosphere before use. Inositol, ammonium persulfate, *p*-phenylenediamine, camphorsulfonic acid (CSA), soldium hydroxide (NaOH), dimethyl sulfoxide (DMSO), ethanol, hexamethylenediisocyanate (HDI), anhydrous tetrahydrofuran (THF), methanol, chloroform, hexane, and camphorsulfonic acid (CSA) were purchased from Aldrich or J&K Scientific Ltd., and used as received.

2.2. Synthesis of amino-capped aniline trimer (AT). AT was synthesized by oxidative coupling reaction of p-phenylenediamine and 2 equiv amounts of aniline by equivalent amounts of $(NH_4)_2S_2O_8$ as the oxidant according to previous report.[32] ^{1}HNMR (400 MHz, DMSO-d_6) δ 6.97 (s, 4H, Ar−H), 6.80 (d, 4H, Ar−H), 6.61 (d, 4H, Ar−H), 5.44 (s, 4H, -NH_2).

2.3. Synthesis of star-shaped PLAs and ESMP. Six-armed star-shaped PLAs were obtained by ring-opening polymerization (ROP). The monomer (LA), 0.1% (molar ratio) initiator ($Sn(Oct)_2$), and co-initiator inositol with various monomer/initiator ratios to control the chain lengths of PLA as reported[20] were weighed and added into a silanized round-bottom flask in a glovebox (MBraunlabstar) purged with N_2. The mixture was sealed and immersed in an oil bath at 110 °C for 48 h. After the reaction, a certain amount of chloroform was added into the flask to dissolve the product. The solution was then precipitated into hexane/methanol (v/v = 95:5) mixture. After centrifugation, the product was dried under reduced pressure in a vacuum oven for 48 h at room temperature. Linear PLA with M_n of 85000 (PLA85k) was also synthesized and used as the control in the following tests.

To prepare the SMPs, the prepolymers, $Sn(Oct)_2$ and HDI were dissolved in anhydrous THF (Figure 1), and the mixture was cast into

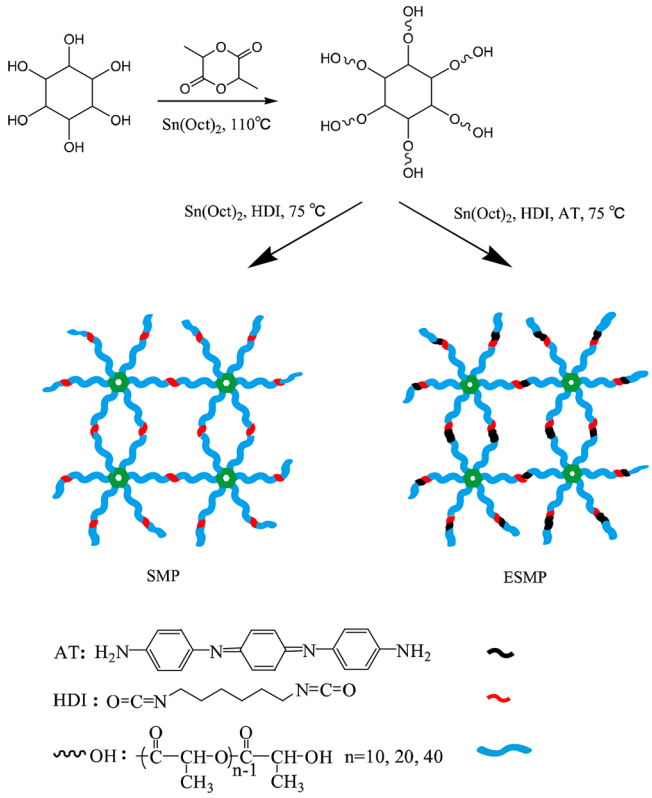

Figure 1. Synthesis scheme of shape memory polymer networks.

a Petri dish, and put into an oven at 75 °C for 24 h. The film of SMP was obtained after the evaporation of THF. The electroactive shape memory polymers (ESMP) were obtained by adding 5 wt % AT and a certain amount of CSA into the reactant mixture before reaction.

To tune thermal-mechanical properties, biodegradability, and shape memory effect, PLAs with various chain lengths were synthesized by changing the molar ratios of monomer/initiator as 60:1, 120:1 and 240:1. Prepolymers were named as P10, P20 and P40 which means the repeating units of the PLA chains was 10, 20 and 40, respectively. The shape memory polymers (SMP) obtained from precursors P10, P20, and P40 were named as PH10, PH20 and PH40, respectively. The electroactive SMPs were named as PH10AT for P10 and PH20AT for P20 after the introduction of AT segment.

2.4. Characterization. FT-IR spectra of prepolymers PLAs, AT and shape memory networks were monitored on a Nicolet 6700 FT-IR spectrometer (Thermo Scientific Instrument) in the range of 4000−

DOI: 10.1021/acsami.5b00191
ACS Appl. Mater. Interfaces 2015, 7, 6772−6781

600 cm^{-1}. The spectra were taken as the average of 32 scans at a resolution of 4 cm^{-1}.

^1H NMR (400 MHz) spectra were recorded at room temperature by using a Bruker Ascend 400 MHz NMR instruments with $CDCl_3$ as the solvent for all PLA samples and as internal standard (δ 7.26 ppm). DMSO-d_6 was used as the solvent for AT and as internal standard (δ 2.50 ppm). Molecular weights of the PLAs were determined by comparing the integrals of methine protons peaks (δ = 5.2 ppm, CH) with those next to the terminated hydroxyl groups (δ = 4.4 ppm, CH) of each arm. Monomer conversion of the LLA was calculated by comparing the integrals of methine protons peak (δ = 5.2 ppm, CH) with the methine protons of lactide (δ = 5.0 ppm, CH). The detailed results of the M_n and monomer conversion are listed in Table 1. The

Table 1. Properties of Star-Shaped PLAs by NMR and GPC

Sample name	Theor mol wt	Mol wt by NMR	M_n by GPC	PDI	Monomer conversion (%)
P10	4500	9000	11100	1.18	95
P20	9000	14000	17000	1.19	95
P40	17000	29000	34000	1.11	99

variation of molecular weights between the theoretical and the experimental ones from NMR and GPC may be due to the trans-esterification reaction during the ring opening polymerization and the incomplete monomer conversion.

Gel permeation chromatography (GPC) measurements were carried out at 40 °C by using Waters instrument, including a column heater equipped with two Waters Styragel columns (HT2 and HT4), a Waters 1525 pump and a Waters 2414 refractive index detector. GPC measurements were conducted in THF at a flow rate of 1 mL/min to determine the average molecular weight and polydispersity index (PDI). Polystyrene standards were used as calibration of molecular weight.

Tensile test was carried out by the MTS Criterion 43 equipped with a 2500 N tension sensor. SMP films were handled according to ASTM D822. The tensile strength, breaking elongation and modulus were obtained at a crosshead rate of 2 mm/min. Each data was represented by average value and standard derivation (SD) ($n \geq 3$).

Cyclic voltammogram (CV) of ESMP was performed on a CHI 660D electrochemical workstation (CH Instruments). An indium tin oxide (ITO) electrode served as working electrode, and an Ag/AgCl and a platinum wire were used as reference and counter electrode, respectively. The ITO glass electrode was immersed into the matrix of reactants of ESMP, then put into a 75 °C oven. A thin polymer film on the ITO glass was formed after the reaction. The scanning rate was 10 mV/s.

Water contact angle test was used to evaluate the surface wettability of the SMPs with a contact angle and surface tension meter (Kino). A drop of Mini-Q water was placed on the surface of the SMP film, and the picture of the water drop was taken. The images were then analyzed by Kino software to obtain the contact angle data. The contact angle of each sample was calculated as the average of six measurements at different points on the films.

The glass-transition temperature (T_g), melting temperature (T_m) and crystallinity (X_c) of PLAs, SMPs and ESMPs were measured by differential scanning calorimetry (DSC) using a TA Q200 DSC with a nitrogen flow at a rate of 50 mL/min. The samples were first heated from room temperature to 200 °C, and equilibrated at 200 °C for 2 min, then cooled down from 200 to −20 °C and heating scan from −20 to 200 °C at a heating rate of 10 °C/min. T_g and T_m were taken from the second heating cycle. X_c was calculated as $X_c = \Delta H_f/\Delta H_f^0$, where ΔH_f is the enthalpy of fusion of the sample, and ΔH_f^0 is the enthalpy of fusion of a 100% crystalline polylactide.

Dynamic mechanical analysis (DMA) in tensile loading mode was used to detect the rubbery modulus of the SMP and ESMP films. Films were cut into 30*6 mm^2 with 0.2−0.3 mm in thickness. Samples were heated from 30 to 110 °C at a rate of 2 °C/min. A 20 μm amplitude and a frequency of 1.0 Hz was applied.

The physiological stability of the SPMs and ESMP was investigated in 0.1 M NaOH solution. The flat films were cut into rectangular discs and recorded the initial weight (m1). The specimens were immersed into vials containing 8 mL NaOH and incubated for a period of time. The specimens were put on a shaker at 37 °C with shaking speed of 100 r/min, and were taken out from the media at certain sampling interval and washed with distilled water. They were then dried at 60 °C oven for 24 h and weighed (m2). Each data was represented as mean ± standard deviation ($n \geq 3$).

$$\text{Weight percentage (\%)} = \text{m2/ml} \times \% \quad (1)$$

Shape memory effect was investigated through exhibiting ability of deformation in various shapes. The specimens with dimensions of 30 mm*6 mm were prepared. The specimens were folded into 180°shape in water at 45 or 55 °C for 1 min, cooled at room temperature for 1 min and returned to 45 or 55 °C water. The angles of the specimens were tested after deformation and recovery, respectively. Cycle was repeated for 3 times. The shape fixity rate (R_f) was used to quantify the ability of fixing the temporary mechanical deformation angle ε_m, stress-free angle $\varepsilon_u(N)$ after unloading. Shape recovery rate (R_r) quantified the ability to restore the permanent angle ε_p (N). A quantitative evaluation of R_f and R_r were calculated by the following equations:

$$R_f(N) = \varepsilon_u(N)\varepsilon_m \times 100\% \quad (2)$$

$$R_r(N) = (\varepsilon_m - \varepsilon_p(N))/(\varepsilon_m - \varepsilon_p(N-1)) \times 100\% \quad (3)$$

N denoted the number of deformation cycle.

2.5. *In vitro* biocompatibility assessment of SMP and ESMP.

2.5.1. C2C12 cell culture. C2C12 myoblast cells were purchased from Shanghai cell bank of Chinese Academy of Sciences. Cells were cultured in Dulbecco's Modified Eagle Medium (DMEM) (GIBCO) supplemented with 10% fetal bovine serum (Gibco) and 100 U/mL penicillin/streptomycin (Gibco), in an incubator at 37 °C in 5% CO_2. When cell confluence reached 90%, C2C12 cells were digested with 0.25% trypsin (Gibco) and passaged. To differentiate into osteocytes, C2C12 cells were treated with differentiation medium which contained 300 ng/mL BMP-2 for 7 days.

2.5.2. Cell proliferation assay. To investigate the cytotoxicity of SMP and ESMP, C2C12 cells were seeded on the PH10, PH20, PH40, PH10AT and PLA85k (M_n= 85k, negative control) films. After sterilized by UV light, films of each sample were fixed in bottom of 24 well plates, and C2C12 cells were seeded at a density of 6000 cells/cm^2. The proliferation of cells on films was evaluated by AlamarBlue assay (Molecular Probes) after cultured for 1, 2, and 3 days, respectively. At each point of detection, the cells were incubated in medium containing 10% (v/v) AlamarBlue dye at 37 °C in 5% CO_2. After 4 h incubated, 100 μL medium of each example was read at 530/600 nm by a SpectraMax fluorescence microplate reader (Molecular Devices). Medium containing 10% (v/v) Alamar blue dye served as a blank.

For live/dead assay, C2C12 cells on films were washed with phosphate buffered saline (PBS) three times and treated with Ethidium homodimer-1 (0.5 μM) and calcein AM (0.25 μM) (Life technologies) for 45 min. Cells were observed under an inverted fluorescent microscope (IX53, Olympus).

2.6. Osteogenic differentiation study of C2C12 cells on SMP and ESMP. Briefly, C2C12 cells were seeded on PH10, PH10AT and PLA85k films in 24 well plates at a density of 10,000 cells/cm^2. After 24 h, the mediums were replaced and the cells were cultured in differentiation mediums for 7 days.

The expression of alkaline phosphatase (ALP) was quantitatively tested at day 7. ALP was extracted and detected with SensoLyte pNPP Alkaline Phosphatase Assay Kit (AnaSpec) according to the manufacturer's instructions. Briefly, cells were digested in 300 μL lysis buffer to release the ALP, and lysate was centrifuged for 10 min at 2500 rmp at 4 °C to obtain the supernatant. Amount of ALP in the cells was normalized against total protein contents.

To visualize the osteogenic differentiation of C2C12 cells on the films, immunofluorescence staining was performed. Films were rinsed

DOI: 10.1021/acsami.5b00191
ACS Appl. Mater. Interfaces 2015, 7, 6772−6781

with PBS, and fixed with 2.5% glutaraldehyde for 15 min, followed by three times PBS washing, and then treated with 0.1% Triton X-100 for 0.5 h and 1% BSA in PBS for 1 h. Then the cells were incubated with Mouse anti-RUNX2 monoclonal antibody (1:500, Abcam) at 4 °C overnight. After being washed for three times with PBS, Alexa flour 488 conjugated secondary antibody (Molecular Probes) was added and incubated for 2 h at room temperature. After three times PBS washing, cells were counterstained with DAPI, and observed under an inverted fluorescence microscopy (IX53, Olympus).

The total RNA of each sample was extracted using Trizol (Invitrogen) by following the manufacturer's instructions. One μg RNA was used to synthesize cDNA using a reverse transcription reagents kit (Fermentas, Thermo scientific). The real-time PCR was carried out according to the protocol and conducted with an Applied Biosystems 7500 Fast Real-time PCR system with the following steps: 95 °C for 30 s, then 40 cycles of 95 °C for 15 s followed by 1 min at 60 °C. There different osteogenic genes were used to assess the osteogenic differentiation: alkaline phosphatase (ALP), Runt-related transcription factor 2 (RUNX2), and type 1 collagen (COL I) along with the housekeeping gene gluteraldehyde phosphate dehydrogenase (Gapdh). Primers were purchased from GeneCopoeia and already proved for quantitative real time PCR. The gene expression was normalized to the housekeeping gene Gapdh in the same sample.

2.7. Statistics. All data were expressed as mean ± standard deviation. The statistical significance was analyzed by a one-way ANOVA test followed by using S−N−K test method. Differences were considered statistically significant when $p < 0.05$.

3. RESULTS AND DISCUSSIONS

3.1. Synthesis of the copolymers. FT-IR spectroscopy was employed to investigate the chemical structure of the polymers. The FT-IR spectra of SMPs and their corresponding precursors are shown in Figure 2A. Compared to curve a1 of P10, the new peaks at 1621 and 1520 cm^{-1} of PH10 were assigned to the −C═O stretching of amide (I) and the stretching vibration combined with out-of-the-plane bending of the −C−N− bond of the urethane group, indicating that the reaction between the hydroxyl group and the isocyanate group took place. Furthermore, no peak at 2280 cm^{-1} assigned to −NCO group was observed, which means that all the HDI was completely incorporated into the PLA. Moreover, the amide (I) peak of PH40, PH20, and PH10 shifted from 1657 to 1641 cm^{-1} to 1621 cm^{-1}, indicating that more hydrogen bonds appeared, because more urethane groups were generated and they had more chances to form hydrogen bonds with each other with decreasing molecular weight of the polylactide.[33] Asymmetric stretching of the −C═O ester of the PLA chain showed an obvious low frequency shift from 1755 cm^{-1} of curve a1 to 1748 cm^{-1} in curves a2, a3, and a4. The red-shift of the −C═O stretching band indicated the hydrogen bond formation between the −C═O in the ester group of PLA chains and urethane groups.

In Figure 2B, comparing to b1 and b3, the disappearance of the characteristic peaks at 3376 and 3196 cm^{-1}, assigned to the terminal -NH_2 in AT, and the appearance of a new peak at 3320 cm^{-1} of -NH- revealed that the aromatic amine -NH_2 in the AT was successfully converted into the imine -NH-.[21] The appearance of a new peak at 1632 cm^{-1} corresponding to the carbonyl for urea linkages demonstrated that the -NH_2 groups were transformed into a urea group after reacting with HDI. Furthermore, the absorption bands at 1595 and 1503 cm^{-1} were assigned to the stretching vibrations of the quinoid ring and the benzenoid ring in AT, respectively. All the data showed that the AT segments were introduced into the polymer network.

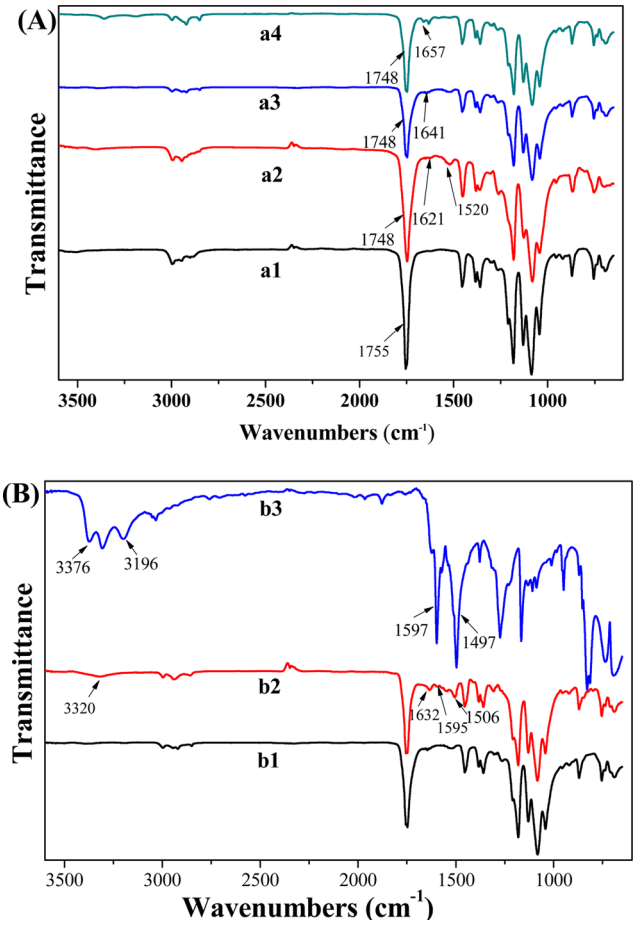

Figure 2. FT-IR spectra of the samples: P10 (a1), PH10 (a2), PH20 (a3), and PH40 (a4) in part A; PH20 (b1), PH20AT (b2), and AT (b3) in part B.

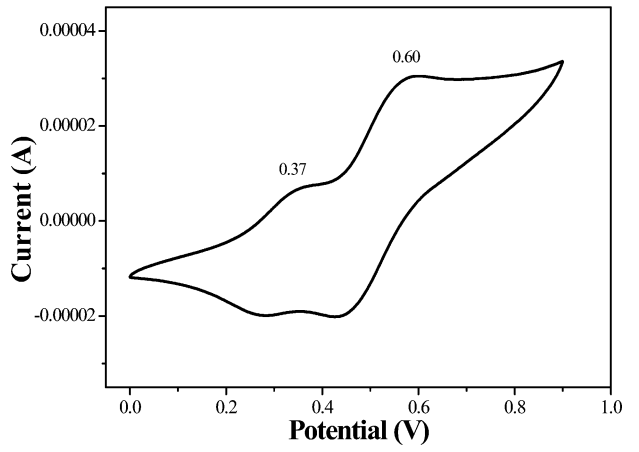

Figure 3. Cyclic voltammogram of the PH10AT film.

The electroactivity of the ESMP was confirmed by cyclic voltammetry (CV), and the result is depicted in Figure 3. There are two well-defined pairs of oxidation/reduction peaks at 0.37 and 0.60 V in the CV curve. The first pair of peaks, at low potential, 0.37 V, is attributed to the reversible transition from the leucoemeraldine state to the emeraldine state. The reversible redox peak at 0.60 V corresponds to the transition from the emeraldine state to the pernigraniline state, which is consistent with previous results.[34]

DOI: 10.1021/acsami.5b00191
ACS Appl. Mater. Interfaces 2015, 7, 6772−6781

Table 2. Thermal Properties of the Polymers[a]

Sample name	T_g (°C)	T_m (°C)	ΔH_m	X_c (%)
P10	51.4	137.7	31.4	33.4
P20	54.9	146.5	36.5	38.8
P40	55.9	155.7	40.9	43.5
PH10	56.4	-	-	-
PH20	58.2	-	-	-
PH40	57.0	148.5	6.8	7.2
PH10AT	56.3	-	-	-
PH20AT	58.2	-	-	-

[a]"-" means not detected. Heat of fusion for the α-forms of PLLA is 94 J/g.[35]

Table 3. Tensile Test Results of the Polymer Networks

Sample name	Stress (MPa)	Modulus (MPa)	Strain (%)
PH10	46.3 ± 0.7	2425.1 ± 236.0	4.9 ± 1.3
PH20	41.6 ± 1.2	1300.6 ± 345.8	10.2 ± 2.3
PH40	40.2 ± 1.4	1006.1 ± 87.2	13.5 ± 4.3
PH10AT	49.3 ± 4.5	1956.7 ± 168.6	3.6 ± 0.4
PLA85k	38.2 ± 2.5	1687.5 ± 142.6	4.3 ± 1.0

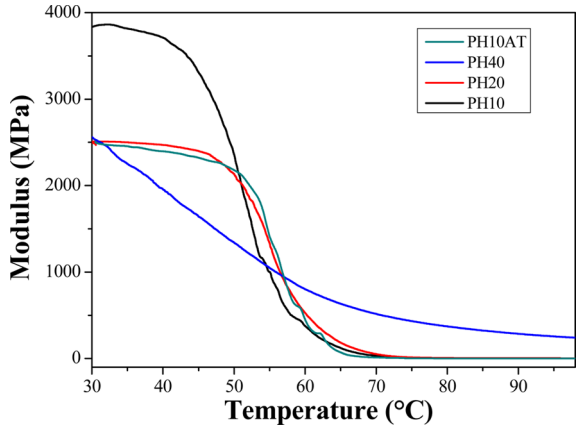

Figure 4. DMA curves of the shape memory networks.

3.2. Thermal properties of the polymers. The thermal properties are also very important for the application of SMP. The glass translation temperature (T_g), melting temperature (T_m), and crystallinity (X_c) of the SMPs are shown in Table 2, and the DSC traces are shown in Figure S1 in the Supporting Information. The T_g of prepolymers was between 51.4 and 55.9 °C, and it increased with increasing molecular weight of PLA chain, because the interactions and entanglements between the PLA chains increased with the lengths of PLA chains. The X_c of the prepolymers increased accordingly with increasing the M_n of PLA, because the branched core inositol hindered the movement of the PLA chain and decreased the formation of crystals of the PLA chain near the branched core.[23] Due to the interruption of the branched core, the formation of the complete crystals was more difficult for the shorter PLA chain length than the longer one. This restricted regular arrangement of the polymer chain to crystallize completely. Therefore, the T_m values of the P10, P20, and P40 increased in order.

T_g of SMPs was between 56.4 and 58.2 °C and increased compared with the corresponding prepolymers, because the chemical cross-linking greatly restricted the movement of the PLA chain. The network structure destroyed the well-organized crystallinity, thus leading to the disappearance of melting peaks

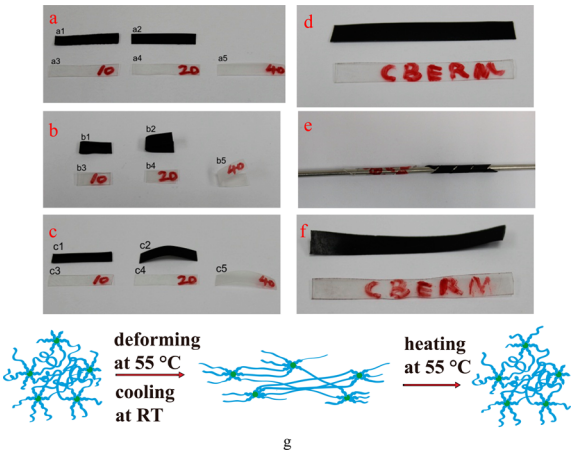

Figure 5. Photos show the shape memory effects of the samples. (a) The initial shape of the samples; (b) Fixed angles of temporary shape; and (c) The residue angles of the samples. Quantitive evaluation of PH10AT (a1, b1, c1), PH20AT (a2, b2, c2), PH10 (a3, b3, c3), PH20 (a4, b4, c4), and PH40 (a5, b5, c5). Qualitative evaluation of PH10 (transparent) and PH10AT (black) in panels d, e, and f. (d) The initial rectangle shape; (e) The spiral shape after fixity; and (f) The final shape of the samples after recovery. All samples were fixed at ambient temperature and recovered at 55 °C water bath; (g) Schematic mechanism of shape memory behavior.

Table 4. Quantitative Shape Memory Properties of the Materials[a]

Sample name	PH10	PH20	PH40	PH10AT	PH20AT
R_{f1} (%)	100	100	77.8	100	80.6
R_{r1} (%)	94.4	98.3	82.1	98.0	87.8
R_{f2} (%)	100	100	73.3	100	100
R_{r2} (%)	100	100	97.9	100	100

[a]R_{f1} shape fixity rate after deformation at 45 °C and fixation at ambient temperature. R_{r1} shape recovery rate at 45 °C. R_{f2} shape fixity rate after deformation at 55 °C and fixation at ambient temperature. R_{r2} shape recovery rate at 55 °C.

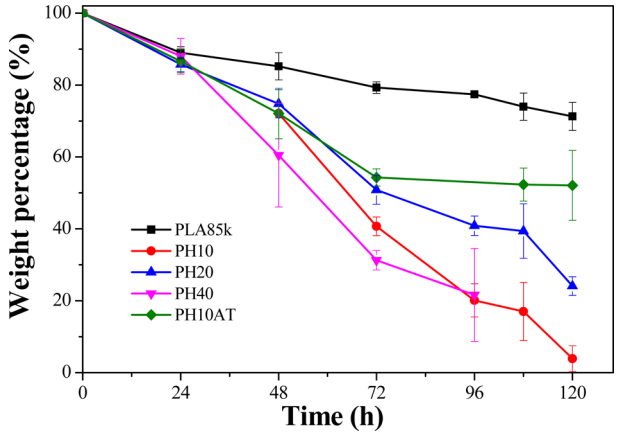

Figure 6. Degradation profile of shape memory polymers.

in DSC curves, which resulted in the optical transparency of the SMPs. The PH40 still retained a small melting peak because of the long chain of PLA which made it easier to get together to crystallize than the other ones. The T_g values of PH10AT and PH20AT were similar to those of PH10 and PH20, meaning that the incorporation of AT into the network hardly affected the thermal properties of the materials.

DOI: 10.1021/acsami.5b00191
ACS Appl. Mater. Interfaces 2015, 7, 6772−6781

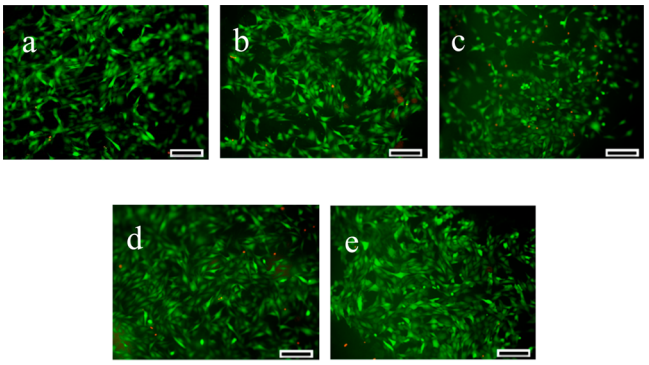

Figure 7. Live/dead staining results of C2C12 cells on: (a) PLA85k, (b) PH10, (c) PH20, (d) PH40, and (e) PH10AT films after 24 h of culture. Scale bar: 200 μm.

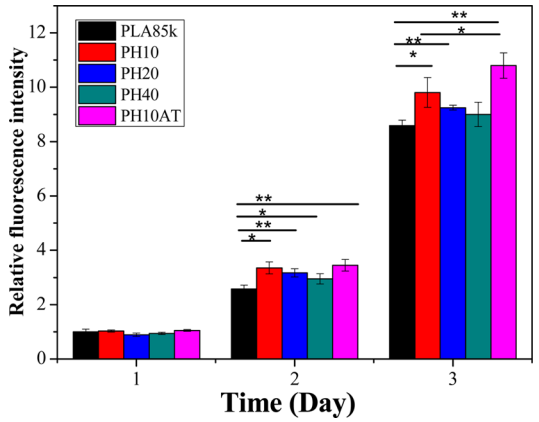

Figure 8. Cell proliferation of PH10, PH20, PH40, and PH10AT at various time points with PLA85k as control. Mean for $n = 4 \pm$ SD. * $p < 0.05$, ** $p < 0.01$.

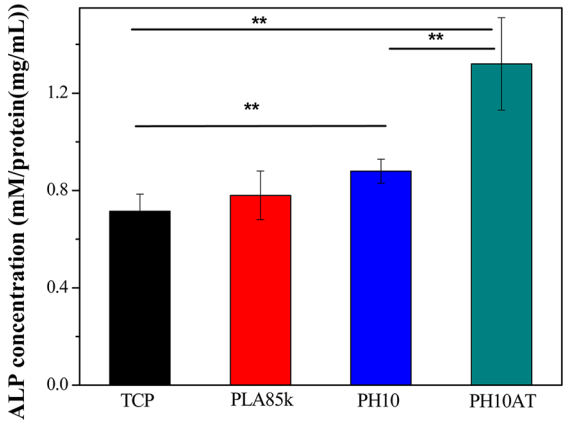

Figure 9. ALP enzyme activity of C2C12 cells on different substrates at day 7. Mean for $n = 4 \pm$ SD. **$p < 0.01$.

3.3. Mechanical properties of the materials. A strong mechanical property of SMP is a requirement for load-bearing application. Generally, all the SMPs showed strong mechanical properties, as shown in Table 3 and in Figure S2 in the Supporting Information. The tensile strengths of PH10, PH20, and PH40 were 46.3, 41.6, and 40.2 MPa, respectively, and the Young's modulus values of PH10, PH20, and PH40 were 2.4, 1.3, and 1.0 GPa, respectively. They were stronger than the SMPs in other reports, in which the modulus was no more than 600 MPa.[36−42] Both the Young's modulus and tensile strength

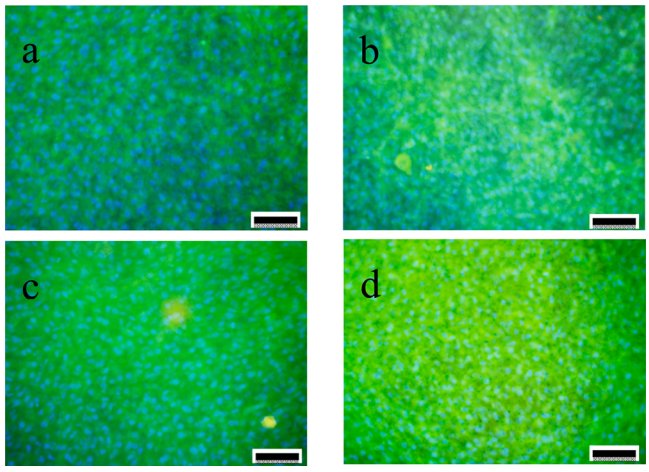

Figure 10. Immunofluorescence staining of C2C12 cells on different films after 7 days of induction. RUNX2 was stained green, and nucleus was stained blue. (a) TCP, (b) PLA85k, (c) PH10, and (d) PH10AT. Scale bar is 100 μm.

of SMP decreased accordingly with decreasing the molecular weight of polylactide, because the increasing chemical cross-linking density enhanced the interaction of the PLA chain and inhibited the slip of the PLA chain. In contrast, the elongation at break of PH10, PH20, and PH40 increased from 4.9% to 13.5% due to the decreased chemical cross-linking density.

In the case of the EMSPs, the hard AT segments destroyed the regular arrangement of the PLA chain after its incorporation in the network. On the other hand, however, AT as the hard segment and the urea groups formed during the reaction could improve the mechanical properties to some degree. These two effects resulted in the higher stress (49.3 MPa), medium modulus (2.0 GPa), and low strain of PH10AT (3.6%).

3.4. Dynamic mechanical properties of the networks. The thermal mechanical properties of the networks were further studied by DMA test. In Figure 4, it showed that the storage modulus values of all the specimens were almost constant at the glassy state and rubbery state except for PH40. The dynamic mechanical response was related to cross-linking density serving as net points which had a significant effect on the modulus of the materials. The PH40 sample had the lowest chemical cross-linking density with the least amount of urethane groups compared to PH10 and PH20 samples. Therefore, PH40 samples showed a relatively lower modulus compared to PH10 and PH20, probably due to the lowest chemical cross-linking density of the sample, and the slipping of the macromolecule chains during the dynamic mechanical experiment. The storage modulus values of PH10AT and PH20 at body temperature were over 2.5 GPa, and the storage modulus of PH10 was even 3.8 GPa, which was higher than the reported toughening polyamide[43] and PLA copolymer reinforced with functionalized multiwall carbon nanotubes,[44] indicating that these SMPs could be used for weight-bearing applications. With temperature increasing, the storage modulus values of PH10, PH20, and PH10AT showed dramatic changes up to 3 orders of magnitude, and the transition temperatures were 52, 55, and 56 °C for PH10, PH20, and PH10AT, respectively. The loss tangent of DMA measurements of PH10, PH20, and PH10AT showed similar transition temperature tendency to DSC results as shown in Figure S3 in the Supporting Information. The sharp changes of the modulus of the materials indicated the sharp triggering of recovery and

DOI: 10.1021/acsami.5b00191
ACS Appl. Mater. Interfaces 2015, 7, 6772−6781

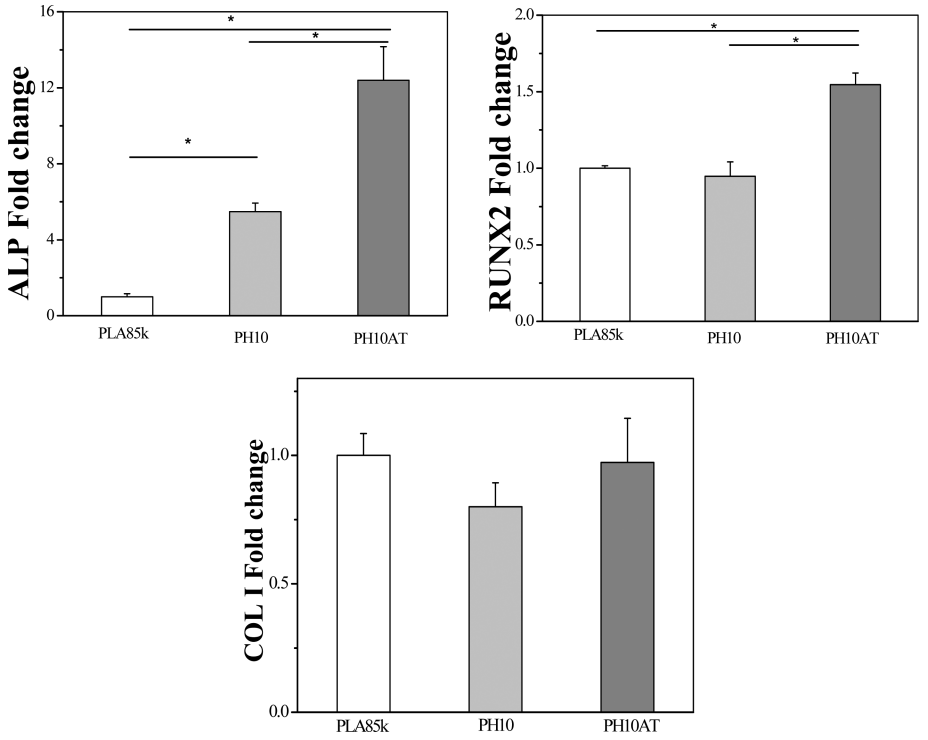

Figure 11. Quantitative analysis of osteogenesis-related gene expression of C2C12 cells on PH10, PH10AT, and PLA85k films in differentiation medium after 7 days of induction. $^{*}p < 0.01$.

fixity. The modulus was a direct sign of the cross-linking density of the polymer which highly influenced the shape recovery process. Although the introduction of the AT segment into PH10 decreased the modulus of PH10, it still kept the platform at a glassy state and a rubbery state. The DMA curve of PH10AT was similar to PH20, which was the indication of the shape memory properties' similarity.

3.5. Shape memory properties of the networks. The shape memory behavior of the fast self-expandable smart materials was examined qualitatively and quantitively. The initial shape was designed as rectangle films. In Figure 5a−c, a simple fold deformation was carried out to demonstrate the shape memory properties for all the samples. All the samples could be fixed completely at room temperature, except for PH40 and PH20AT. The deformed samples recovered to initial shape at 55 °C completely in 2−3 s except PH40 and PH20AT. It was obviously faster than the reported recovery time over several minutes, even several hours.[6,38,39,45]

To further evaluate the potential application of SMPs as strong self-expandable materials, we made a complex mode to show the shape memory process. The straight film (thickness in 0.15 mm) was wreathed around a metallic cylinder with a diameter of 2.98 mm, as shown in Figure 5e. The outer diameters of PH10 and PH10AT were 3.35 mm and 3.54 mm, respectively. The recovery proccesses of both samples at 55 °C were finished in 20 s completely, as shown in the video in the Supporting Information, indicating that these SMPs could be used for complex self-expandable materials. The PH10 and PH10AT showed similar behavior at 45 °C with longer recovery time (in 50 s).

In Table 4, it showed R_f and R_r results in the third cycle at different deformation and recovery temperatures (45 and 55 °C). For the process at 45 °C, R_{f1} of PH10 and PH20 both reached to 100%, and R_{r1} to 94.4% and 98.3%, respectively, which was much better than the no more than 86% values reported in the literature.[8,37,46] Nevertheless, R_{f1} and R_{r1} of sample PH40 were only 77.8% and 82.1%, respectively. This could be led by the different cross-linking densities which indicated the mechanism of the shape memory effect. After the addition of AT, the hard segments weaken the shape memory effect of PH20 at 45 °C. This may be attributed to the rigid AT segment hindering the movement of PLA chains at low temperature (45 °C). When rising the temperature to 55 °C, it resulted in more internal energy and more flexible switch domains to deform and trigger the shape recovery sharply and completely. All the samples showed 100% R_{f2} and R_{r2}, except PH40. But PH40 still exhibited the improvement in shape memory properties at 55 °C. No matter at 45 or 55 °C, PH20 and PH10AT showed similar shape memory behavior. This result was in accordance with the DMA test.

The above results showed the SMP and ESMP exhibited good shape memory properties, such as fast recovery speed, good recovery, and excellent fixity at a temperature close to the physiological one compared to some references.[2,6,38,47−51] The strong SMPs have great potential application over other reported weak SMPs for the requirement of weight-bearing property.[41]

We further assumed the mechanism to elucidate the shape memory proccess, as shown in Figure 5g. The chains of PLA serving as switching units are homogeneous at ambient environment, and the rigid core myo-inosital molecules anchor in the PLA chains tightly. The SMP or ESMP was deformed on demand after heating and cooled down to keep the deformation. The chains of PLA were arranged along the direction of stress and fixed at the same time. Upon heating, the PLA chains were activated at once and moved to the original place. Then the SMP or ESMP recovered to the initial shape.

DOI: 10.1021/acsami.5b00191
ACS Appl. Mater. Interfaces 2015, 7, 6772−6781

3.6. Degradation of the materials. Degradation properties are quite important for biomedical polymers. Degradation profiles of the SMP samples in 0.1 M NaOH solution were presented in Figure 6. The PH40 showed the faster degradation rate than PH10 and PH20, because the density of cross-linking regulated the degradation of SMP effectively. PH40 with the lowest cross-linking density was much more easily hydrolyzed; thus, it degraded the fastest. Although PH10 had a higher degree of chemical cross-linking, it exhibited faster degradation rate than PH20. This could be assigned to the hydrophilic -NH−COO- group allowing easy access to hydrolytically labile substrate to accelerate the degradation.[52] PH10AT exhibited relatively slow degradation compared with PH10. This was attributed to the resistant effect to degradation of the hard segment. AT existing in the PLA chain inhibited the movement of the soft segment to get access to hydrolysis. Nonetheless, the PH10AT still degraded faster than the pure PLA85k due to the presence of the urethane group.

3.7. Wettability of the SMPs. A contact angle test was carried out to verify the hydrophobicity of the materials as shown in Figure S4 in the Supporting Information. The contact angle of water of PH10, PH20, and PH40 increases accordingly, and they are lower than that of PLA85k, indicating that they are more hydrophilic compared to PLA85k due to the formation of urethane groups in the copolymers. The PH10AT exhibits the lowest water contact angle about 72°, meaning that the introduction of AT to PH10 greatly improves the hydrophilicity of PH10AT, which is more suitable for cell adhesion and cell function.

3.8. Cell adhesion and proliferation on SMP and ESMP films. The *in vitro* biocompatibility of SMP and ESMP was measured by the C2C12 cell adhesion and proliferation on these polymer films. In this study, C2C12 cells were seeded on PH10, PH20, PH40, PH10AT, and PLA films and cultured for 1 day to evaluate the cell viability and for 3 days to determine the cell proliferation.

To visualize the cell adhesion and viability, after 24 h of culture, the live/dead staining of C2C12 cells on different substrates was performed. On both SMP and ESMP films, most of the cells were found to be alive (stained with green) and displayed spindle-like shaped morphologies which were similar to cells cultured on PLA (Figure 7 (a)). These results demonstrated that both SMP and ESMP showed a good biocompatibility and no side-effects on cell adhesion and morphology.

After being cultured for 24 h, cells on PH10 and PH10AT films showed higher cell number than that on PLA films, as shown in Figure 8, and cells on PH20 and PH40 films had cells number equivalent to that on PLA films, which indicated that the cells adhered well on SMP and ESMP films compared with PLA films. After 2 days of culturing, cells on PH10, PH20, PH40, and PH10AT films all exhibited significantly higher proliferation rates than that on PLA85k films ($p < 0.05$). On days 2 and 3, the cell proliferation of C2C12 myoblasts on PH10 films is higher than that on PH40 ($P < 0.05$), which might be due to the higher wettability of PH10 sample that is more suitable for cell proliferation. Moreover, for the third day, the cells cultured on PH10 (1.14 times, $p < 0.05$), PH20 (1.08 times, $p < 0.01$), PH40 (1.05 times, $p > 0.05$), and PH10AT (1.26 times, $p < 0.01$) films showed higher proliferation rates than that on PLA85k films. Furthermore, the cells on PH10AT films displayed significantly higher number than PH10 films ($p < 0.05$), indicating that the introduction of electroactive AT segments into SMP could significantly enhance the proliferation of C2C12 cells compared to that of SMP and PLA, because the doped ESMP enhanced the chemical and energy exchange between cells and surroundings for its electroactivity and the AT segment enhanced the wettability of PH10AT.

3.9. Influence of SMP and ESMP on the osteogenic differentiation of C2C12 cells. The strong mechanical properties of SMP and ESMP demonstrated the potential application in bone tissue engineering. C2C12 cells are chosen because they are electrically sensitive and can be differentiated into osteocytes, to investigate the effect of ESMP on osteogenic differentiation *in vitro*. After being cultured 7 days, ALP enzyme activity, immunofluorescence staining, and qRT-PCR were performed for quantitative and qualitative assay.

ALP is an early marker of osteogenic differentiation, and the enormous amount of ALP mRNA and ALP enzyme activity demonstrates the beginning of osteogenic differentiation.[53] Due to their higher proliferation rate, PH10 and PH10AT films were used to investigate their differentiation capacity. Figure 9 showed the ALP enzyme activity after 7 days of induction on different substrates. The ALP enzyme activity of C2C12 cells on PH10 sample was higher than that of PLA85k and TCP ($p < 0.05$), indicating that the PH10 can promote the ALP activity compared to PLA. Moreover, the ALP activity of C2C12 myoblasts on PH10AT significantly increased compared to PLA and TCP, and even to PH10, suggesting that the osteogenic differentiation of C2C12 cells on the electroactive PH10AT substrate was much better than other substrates, including tissue culture polystyrene.

To visualize osteogenic differentiation of C2C12 myoblasts, the immunofluorescence staining of RUNX2, one of the osteogenic markers, was performed after 7 days of induction. Figure 10 showed staining results of the cells on TCP, PH10, PLA, and PH10AT, respectively. The fluorescence intensity of cells on PH10AT substrates exhibited a much brighter fluorescence, which indicated that the expression of RUNX2 protein in C2C12 cells on PH10AT films was much higher than those of other films, owing to the enhanced differentiation and proliferation rate of C2C12 cells into osteogenic lineage.

Besides ALP enzyme activity assay and immunofluorescence staining, qRT-PCR was also performed to analyze osteogenic differentiation of C2C12 myoblasts on the mRNA level. Three osteogenesis-related genes (ALP, RUNX2, and COL I) were investigated. The relative expression levels of these three genes in C2C12 cells inducted for 7 days on PH10 and PH10AT films are shown in Figure 11. The gene expression of ALP on the electroactive PH10AT films was conspicuously up-regulated (12 times that of PLA85k films and 6 times that of PH10 films) after 7 days of induction ($p < 0.05$) (Figure 11), which agreed well with the ALP enzyme activity results and proved the significantly promoting effect on C2C12 osteogenic differentiation on PH10AT substrates. Meanwhile, the gene expression of RUNX2 (a member of the runt homology domain family of transcription factors that associated with osteogenic differentiation[54]) and COL I (the main extracellular matrix protein in osteoblast[55]) were enhanced after induction on PH10AT films, compared with that on PH10 (Figure 11). These results were explained by the thought that the charged surface stimulates some cell signaling pathways that involved ALP expression, and the secretion of RUNX2 and COL I. The data from qRT-PCR, ALP enzyme activity assay, as well as immunofluorescence staining all suggest that PH10AT can significantly promote C2C12 cells osteogenic differentiation

DOI: 10.1021/acsami.5b00191
ACS Appl. Mater. Interfaces 2015, 7, 6772−6781

compared with PLA85k and PH10, indicating that electroactive PH10AT is a good candidate for bone tissue engineering.

4. CONCLUSIONS

The strong electroactive degradable shape memory polymers based on branched polylactide with inositol as core and amine-capped aniline trimer were successfully synthesized. The mechanical properties of SMPs and ESMPs were tunable and in the range of GPa under body temperature. The SMP (PH10 and PH20) and ESMP demonstrated excellent shape memory properties: short recovery time, high recovery ratio, and fixity ratio. The cell proliferation assay showed that the electroactive ESMP possessed good biocompatibility and greatly enhanced the proliferation of C2C12 cells compared to SMPs and PLA85k. In addition, the ESMP significantly improved the osteogenic differentiation of C2C12 cells compared to PH10 and PLA85k. These novel biocompatible SMPs and electroactive SMPs with strong mechanical properties, tunable degradability, and electroactivity are excellent candidates for bone tissue engineering.

■ ASSOCIATED CONTENT

Ⓢ Supporting Information

Representative DSC traces, mechanical curves, loss tangent of DMA measurements and contact angle values of samples, and video of shape memory property of the materials. This material is available free of charge via the Internet at http://pubs.acs.org.

■ AUTHOR INFORMATION

Corresponding Authors

*Tel.:+86-29-83395361. Fax: +86-29-83395131. E-mail: baoling@mail.xjtu.edu.cn (B.G.).

*Tel.:+86-29-83395361. Fax: +86-29-83395131. E-mail: mapx@umich.edu (P.M.).

Author Contributions

$^{\nabla}$M.X. and L.W. contributed equally.

Notes

The authors declare no competing financial interest.

■ ACKNOWLEDGMENTS

The National Natural Science Foundation of China (grant number: 21304073) and Xi'an Jiaotong University are acknowledged for financial support of this work.

■ REFERENCES

(1) Lendlein, A.; Langer, R. Biodegradable, Elastic Shape-Memory Polymers for Potential Biomedical Applications. *Science* **2002**, *296*, 1673−1676.

(2) Yakacki, C. M.; Shandas, R.; Lanning, C.; Rech, B.; Eckstein, A.; Gall, K. Unconstrained Recovery Characterization of Shape-Memory Polymer Networks for Cardiovascular Applications. *Biomaterials* **2007**, *28*, 2255−2263.

(3) Xue, L.; Dai, S.; Li, Z. Synthesis and Characterization of Elastic Star Shape-Memory Polymers as Self-Expandable Drug-Eluting Stents. *J. Mater. Chem.* **2012**, *22*, 7403−7411.

(4) Baer, G.; Wilson, T.; Maitland, D.; Matthews, D. Shape Memory Polymer Neurovascular Stents.: 483. *J. Invest. Med.* **2006**, *54*, S162.

(5) Xu, J.; Song, J. High Performance Shape Memory Polymer Networks Based on Rigid Nanoparticle Cores. *Proc. Natl. Acad. Sci. U.S.A.* **2010**, *107*, 7652−7657.

(6) Zheng, X.; Zhou, S.; Li, X.; Weng, J. Shape Memory Properties of Poly (D, L-Lactide)/Hydroxyapatite Composites. *Biomaterials* **2006**, *27*, 4288−4295.

(7) Guo, B. L.; Ma, P. X. Synthetic Biodegradable Functional Polymers for Tissue Engineering—A Brief Review. *Sci. China Chem.* **2014**, *57*, 490−500.

(8) Peponi, L.; Navarro-Baena, I.; Sonseca, A.; Gimenez, E.; Marcos-Fernandez, A.; Kenny, J. M. Synthesis and Characterization of PCL−PLLA Polyurethane with Shape Memory Behavior. *Eur. Polym. J.* **2013**, *49*, 893−903.

(9) Knight, P. T.; Lee, K. M.; Qin, H.; Mather, P. T. Biodegradable Thermoplastic Polyurethanes Incorporating Polyhedral Oligosilsesquioxane. *Biomacromolecules* **2008**, *9*, 2458−2467.

(10) Taji, T.; Takahashi, S.; Shinozaki, K. Inositols and Their Metabolites in Abiotic and Biotic Stress Responses. *Biology of Inositols and Phosphoinositides*; Springer: 2006; pp 239−264.

(11) Guo, B. L.; Finne-Wistrand, A.; Albertsson, A. C. Biodegradable and Electrically Conducting Polymers for Biomedical Applications. *Prog. Polym. Sci.* **2013**, *38*, 1263−1286.

(12) Li, L.; Ge, J.; Wang, L.; Guo, B. L.; Ma, P. X. Electroactive Nanofibrous Biomimetic Scaffolds by Thermally Induced Phase Separation. *J. Mater. Chem. B* **2014**, *2*, 6119−6130.

(13) Runge, M. B.; Dadsetan, M.; Baltrusaitis, J.; Ruesink, T.; Lu, L.; Windebank, A. J.; Yaszemski, M. J. Development of Electrically Conductive Oligo (Polyethylene Glycol) Fumarate-Polypyrrole Hydrogels for Nerve Regeneration. *Biomacromolecules* **2010**, *11*, 2845−2853.

(14) Shao, S.; Zhou, S.; Li, L.; Li, J.; Luo, C.; Wang, J.; Li, X.; Weng, J. Osteoblast Function on Electrically Conductive Electrospun Pla/Mwcnts Nanofibers. *Biomaterials* **2011**, *32*, 2821−2833.

(15) Li, L. C.; Ge, J.; Guo, B. L.; Ma, P. X. In Situ Forming Biodegradable Electroactive Hydrogels. *Polym. Chem.* **2014**, *5*, 2880−2890.

(16) Xu, H.; Holzwarth, J. M.; Yan, Y.; Xu, P.; Zheng, H.; Yin, Y.; Li, S.; Ma, P. X. Conductive Ppy/PDLLA Conduit for Peripheral Nerve Regeneration. *Biomaterials* **2014**, *35*, 225−235.

(17) Green, R. A.; Lovell, N. H.; Wallace, G. G.; Poole-Warren, L. A. Conducting Polymers for Neural Interfaces: Challenges in Developing an Effective Long-Term Implant. *Biomaterials* **2008**, *29*, 3393−3399.

(18) Wu, Y.; Guo, B. L.; Ma, P. X. Injectable Electroactive Hydrogels Formed Via Host−Guest Interactions. *ACS Macro Lett.* **2014**, *3*, 1145−1150.

(19) Guo, B. L.; Finne-Wistrand, A.; Albertsson, A.-C. Electroactive Hydrophilic Polylactide Surface by Covalent Modification with Tetraaniline. *Macromolecules* **2012**, *45*, 652−659.

(20) Guo, B. L.; Finne-Wistrand, A.; Albertsson, A.-C. Molecular Architecture of Electroactive and Biodegradable Copolymers Composed of Polylactide and Carboxyl-Capped Aniline Trimer. *Biomacromolecules* **2010**, *11*, 855−863.

(21) Guo, B. L.; Finne-Wistrand, A.; Albertsson, A.-C. Degradable and Electroactive Hydrogels with Tunable Electrical Conductivity and Swelling Behavior. *Chem. Mater.* **2011**, *23*, 1254−1262.

(22) Cui, H.; Shao, J.; Wang, Y.; Zhang, P.; Chen, X.; Wei, Y. PLA-PEG-PLA and Its Electroactive Tetraaniline Copolymer as Multi-Interactive Injectable Hydrogels for Tissue Engineering. *Biomacromolecules* **2013**, *14*, 1904−1912.

(23) Guo, B. L.; Finne-Wistrand, A.; Albertsson, A.-C. Enhanced Electrical Conductivity by Macromolecular Architecture: Hyperbranched Electroactive and Degradable Block Copolymers Based on Poly (ε-Caprolactone) and Aniline Pentamer. *Macromolecules* **2010**, *43*, 4472−4480.

(24) Ma, X. J.; Ge, J.; Li, Y.; Guo, B. L.; Ma, P. X. Nanofibrous Electroactive Scaffolds from a Chitosan-Graft-Aniline Tetramer by Electrospinning for Tissue Engineering. *RSC Adv.* **2014**, *4*, 13652−13661.

(25) Huang, L. H.; Hu, J.; Lang, L.; Wang, X.; Zhang, P. B.; Jing, X. B.; Wang, X. H.; Chen, X. S.; Lelkes, P. I.; MacDiarmid, A. G.; Wei, Y. Synthesis and Characterization of Electroactive and Biodegradable Aba Block Copolymer of Polylactide and Aniline Pentamer. *Biomaterials* **2007**, *28*, 1741−1751.

(26) Huang, L. H.; Zhuang, X. L.; Hu, J.; Lang, L.; Zhang, P. B.; Wang, Y. S.; Chen, X. S.; Wei, Y.; Jing, X. B. Synthesis of

DOI: 10.1021/acsami.5b00191
ACS Appl. Mater. Interfaces 2015, 7, 6772−6781

Biodegradable and Electroactive Multiblock Polylactide and Aniline Pentamer Copolymer for Tissue Engineering Applications. *Biomacromolecules* **2008**, *9*, 850−858.
(27) Guo, B. L.; Finne-Wistrand, A.; Albertsson, A.-C. Simple Route to Size-Tunable Degradable and Electroactive Nanoparticles from the Self-Assembly of Conducting Coil−Rod−Coil Triblock Copolymers. *Chem. Mater.* **2011**, *23*, 4045−4055.
(28) Zhao, W.; Glavas, L.; Odelius, K.; Edlund, U.; Albertsson, A.-C. Facile and Green Approach Towards Electrically Conductive Hemicellulose Hydrogels with Tunable Conductivity and Swelling Behavior. *Chem. Mater.* **2014**, *26*, 4265−4273.
(29) Hardy, C. G.; Islam, M. S.; Gonzalez-Delozier, D.; Morgan, J. E.; Cash, B.; Benicewicz, B. C.; Ploehn, H. J.; Tang, C. Converting an Electrical Insulator into a Dielectric Capacitor: End-Capping Polystyrene with Oligoaniline. *Chem. Mater.* **2013**, *25*, 799−807.
(30) Lu, W.; Sheng Meng, X.; Yuan Wang, Z. Electrochemical Behavior of a New Electroactive Polyimide Derived from Aniline Trimer. *J. Polym. Sci., Part A: Polym. Chem.* **1999**, *37*, 4295−4301.
(31) Wang, Z. Y.; Yang, C.; Gao, J. P.; Lin, J.; Meng, X.; Wei, Y.; Li, S. Electroactive Polyimides Derived from Amino-Terminated Aniline Trimer. *Macromolecules* **1998**, *31*, 2702−2704.
(32) Wei, Y.; Yang, C.; Ding, T. A One-Step Method to Synthesize N,N′-Bis(4′-Aminophenyl)-1,4-Quinonenediimine and Its Derivatives. *Tetrahedron Lett.* **1996**, *37*, 731−734.
(33) Wang, Z.; Hou, Z. Y.; Wang, Y. F. Fluorinated Waterborne Shape Memory Polyurethane Urea for Potential Medical Implant Application. *J. Appl. Polym. Sci.* **2013**, *127*, 710−716.
(34) Bhadani, S. N.; Gupta, M. K.; Gupta, S. K. S. Cyclic Voltammetry and Conductivity Investigations of Polyaniline. *J. Appl. Polym. Sci.* **1993**, *49*, 397−403.
(35) Sawai, D.; Tsugane, Y.; Tamada, M.; Kanamoto, T.; Sungil, M.; Hyon, S. H. Crystal Density and Heat of Fusion for a Stereo-Complex of Poly (L-Lactic Acid) and Poly (D-Lactic Acid). *J. Polym. Sci., Part B: Polym. Phys.* **2007**, *45*, 2632−2639.
(36) Bai, Y.; Jiang, C.; Wang, Q.; Wang, T. A Novel High Mechanical Strength Shape Memory Polymer Based on Ethyl Cellulose and Polycaprolactone. *Carbohydr. Polym.* **2013**, *96*, 522−527.
(37) Jung, Y. C.; Kim, J. H.; Hayashi, T.; Kim, Y. A.; Endo, M.; Terrones, M.; Dresselhaus, M. S. Fabrication of Transparent, Tough, and Conductive Shape-Memory Polyurethane Films by Incorporating a Small Amount of High-Quality Graphene. *Macromol. Rapid Commun.* **2012**, *33*, 628−634.
(38) Balasubramanian, A.; Morhard, R.; Bettinger, C. J. Shape-Memory Microfluidics. *Adv. Funct. Mater.* **2013**, *23*, 4832−4839.
(39) Yakacki, C. M.; Shandas, R.; Safranski, D.; Ortega, A. M.; Sassaman, K.; Gall, K. Strong, Tailored, Biocompatible Shape-Memory Polymer Networks. *Adv. Funct. Mater.* **2008**, *18*, 2428−2435.
(40) Lendlein, A.; Zotzmann, J. r.; Feng, Y.; Alteheld, A.; Kelch, S. Controlling the Switching Temperature of Biodegradable, Amorphous, Shape-Memory Poly (Rac-Lactide) Urethane Networks by Incorporation of Different Comonomers. *Biomacromolecules* **2009**, *10*, 975−982.
(41) Xue, L.; Dai, S.; Li, Z. Biodegradable Shape-Memory Block Co-Polymers for Fast Self-Expandable Stents. *Biomaterials* **2010**, *31*, 8132−8140.
(42) Bao, M.; Lou, X.; Zhou, Q.; Dong, W.; Yuan, H.; Zhang, Y. Electrospun Biomimetic Fibrous Scaffold from Shape Memory Polymer of PDLLA-co-TMC for Bone Tissue Engineering. *ACS Appl. Mater. Interfaces* **2014**, *6*, 2611−2621.
(43) Zhang, W.; Chen, L.; Zhang, Y. Surprising Shape-Memory Effect of Polylactide Resulted from Toughening by Polyamide Elastomer. *Polymer* **2009**, *50*, 1311−1315.
(44) Amirian, M.; Chakoli, A. N.; Sui, J.; Cai, W. Enhanced Shape Memory Effect of Poly (L-Lactide-Co-ε-Caprolactone) Biodegradable Copolymer Reinforced with Functionalized Mwcnts. *J. Polym. Res.* **2012**, *19*, 1−10.
(45) Venkatraman, S. S.; Tan, L. P.; Joso, J. F. D.; Boey, Y. C. F.; Wang, X. Biodegradable Stents with Elastic Memory. *Biomaterials* **2006**, *27*, 1573−1578.
(46) Xie, T. Tunable Polymer Multi-Shape Memory Effect. *Nature* **2010**, *464*, 267−270.
(47) Chen, M.-C.; Tsai, H.-W.; Chang, Y.; Lai, W.-Y.; Mi, F.-L.; Liu, C.-T.; Wong, H.-S.; Sung, H.-W. Rapidly Self-Expandable Polymeric Stents with a Shape-Memory Property. *Biomacromolecules* **2007**, *8*, 2774−2780.
(48) Miaudet, P.; Derré, A.; Maugey, M.; Zakri, C.; Piccione, P. M.; Inoubli, R.; Poulin, P. Shape and Temperature Memory of Nanocomposites with Broadened Glass Transition. *Science* **2007**, *318*, 1294−1296.
(49) Garle, A.; Kong, S.; Ojha, U.; Budhlall, B. M. Thermoresponsive Semicrystalline Poly(Epsilon-Caprolactone) Networks: Exploiting Cross-Linking with Cinnamoyl Moieties to Design Polymers with Tunable Shape Memory. *ACS Appl. Mater. Interfaces* **2012**, *4*, 645−657.
(50) Lin, T.; Tang, Z.; Guo, B. New Design Strategy for Reversible Plasticity Shape Memory Polymers with Deformable Glassy Aggregates. *ACS Appl. Mater. Interfaces* **2014**, *6*, 21060−21068.
(51) Pilate, F.; Mincheva, R.; De Winter, J.; Gerbaux, P.; Wu, L.; Todd, R.; Raquez, J.-M.; Dubois, P. Design of Multistimuli-Responsive Shape-Memory Polymer Materials by Reactive Extrusion. *Chem. Mater.* **2014**, *26*, 5860−5867.
(52) Dey, J.; Xu, H.; Shen, J.; Thevenot, P.; Gondi, S. R.; Nguyen, K. T.; Sumerlin, B. S.; Tang, L.; Yang, J. Development of Biodegradable Crosslinked Urethane-Doped Polyester Elastomers. *Biomaterials* **2008**, *29*, 4637−4649.
(53) Katagiri, T.; Yamaguchi, A.; Komaki, M.; Abe, E.; Takahashi, N.; Ikeda, T.; Rosen, V.; Wozney, J. M.; Fujisawa-Sehara, A.; Suda, T. Bone Morphogenetic Protein-2 Converts the Differentiation Pathway of C2C12 Myoblasts into the Osteoblast Lineage. *J. Cell Biol.* **1994**, *127*, 1755−1766.
(54) Lee, K.-S.; Kim, H.-J.; Li, Q.-L.; Chi, X.-Z.; Ueta, C.; Komori, T.; Wozney, J. M.; Kim, E.-G.; Choi, J.-Y.; Ryoo, H.-M. Runx2 Is a Common Target of Transforming Growth Factor B1 and Bone Morphogenetic Protein 2, and Cooperation between Runx2 and Smad5 Induces Osteoblast-Specific Gene Expression in the Pluripotent Mesenchymal Precursor Cell Line C2C12. *Mol. Cell. Biol.* **2000**, *20*, 8783−8792.
(55) Kalajzic, I.; Staal, A.; Yang, W.-P.; Wu, Y.; Johnson, S. E.; Feyen, J. H.; Krueger, W.; Maye, P.; Yu, F.; Zhao, Y. Expression Profile of Osteoblast Lineage at Defined Stages of Differentiation. *J. Biol. Chem.* **2005**, *280*, 24618−24626.

DOI: 10.1021/acsami.5b00191
ACS Appl. Mater. Interfaces 2015, 7, 6772−6781